


Cite this: *RSC Adv.*, 2018, **8**, 26691Received 4th May 2018  
Accepted 18th July 2018

DOI: 10.1039/c8ra03840f

rsc.li/rsc-advances

## CuFe<sub>2</sub>S<sub>3</sub> as electrode material for Li-ion batteries

Emmanuel Anger, Antoine Maignan, Tristan Barbier and Valerie Pralong \*

Electrochemical performances of the isocubanite CuFe<sub>2</sub>S<sub>3</sub> tested as electrode material for Li-ion batteries have been investigated. A first discharge capacity of 860 mA h g<sup>-1</sup> shows a conversion process leading to Li<sub>2</sub>S, copper and iron nanoparticles. Interestingly, a reversible capacity of 560 mA h g<sup>-1</sup> at 1.5 V is demonstrated with good cyclability up to 30 cycles.

Because of their low cost and high theoretical capacity, metal sulfides are considered as one potential future electrode material for Li-ion batteries (LIBs). Therefore, numerous materials containing sulfur have been studied in the last decades as cathode materials such as MnS,<sup>1</sup> Cu<sub>x</sub>S,<sup>2</sup> CoS,<sup>3</sup> NiS,<sup>4</sup> and Fe<sub>x</sub>S.<sup>5</sup> Moreover, some metal sulfides have also been reported as anode materials such as SnS<sub>2</sub> (ref. 6) and ZnS.<sup>7</sup> Their reductions happen through a conversion process at low working voltage (under 1 V vs. Li<sup>+</sup>/Li) leading to formation of lithium sulfide and native metal.<sup>8</sup>

Among the conversion materials based on transition metal sulfur, copper and iron are the most cost effective, light and non-toxic elements that one can find. For these reasons, Cu<sub>x</sub>S<sup>2,9,10</sup> and Fe<sub>x</sub>S<sup>5,11,12</sup> have been well studied in the last few decades using either polymer or liquid electrolytes. From these studies, we know that the reduction of these transition metal sulfides forms nanoparticles of metal and lithium sulfides through a conversion process.<sup>8</sup> Therefore, recent articles have been focusing on improving the electrochemical performance of metal sulfides by using hydrothermal,<sup>11</sup> sol-gel<sup>13</sup> or ball-milling<sup>14</sup> synthetic methods.

Copper/iron sulfides are interesting electrode materials because of their higher electrical conductivity and electrochemical activity compared to monometal sulfides.<sup>15</sup> In recent years, only a few studies have been reported on chalcopyrite CuFeS<sub>2</sub>, first as a cathode in a primary battery<sup>16</sup> then as an anode and cathode in a secondary battery.<sup>15,17,18</sup> Different synthetic routes from solvothermal to nanocrystal growth and different electrolytes have proven the potential of chalcopyrite as electrode material for lithium batteries.

Herein, we report the electrochemical performance of the cubic cubanite, so-called isocubanite CuFe<sub>2</sub>S<sub>3</sub>, as the first ternary metal sulfide electrode material for lithium batteries. This Li/CuFe<sub>2</sub>S<sub>3</sub> system exhibits a high reversibility (up to 560 mA h g<sup>-1</sup> at C/20/Li) and a good cyclability over

30 cycles. *Ex situ* X-ray diffraction (XRD)<sup>†</sup> measurements allow a better understanding of the electrochemical mechanism.

The cubanite CuFe<sub>2</sub>S<sub>3</sub> phase crystallizes within an orthorhombic structure (space group: *Pcmn*), with *a* = 6.467 Å, *b* = 11.110 Å and *c* = 6.230 Å.<sup>19</sup> When the orthorhombic CuFe<sub>2</sub>S<sub>3</sub> is heated above 473 K, an irreversible structural transition occurs and CuFe<sub>2</sub>S<sub>3</sub> adopts a cubic structural type (space group: *F43m*, *a* = 5.296 Å). It should be noticed that cubanite and its cubic polymorph isocubanite are usually found in their natural states intimately intergrown with other sulfides such as chalcopyrite and pyrrhotite. Synthesis of isocubanite CuFe<sub>2</sub>S<sub>3</sub> has been first reported by S. Pareek *et al.*<sup>20</sup> In this paper, we chose a synthetic protocol recently described by Barbier *et al.*<sup>21</sup> Following precursors: Cu (99.0%), Fe (99.5%), and S (99.5%) from Alfa Aesar, were mixed in the appropriate ratio. After sealing the cold pressed powder in a silica tube, the latter was heated at 873 K for 48 h. The room temperature powder X-ray diffraction pattern of CuFe<sub>2</sub>S<sub>3</sub> (depicted in Fig. 1) shows that CuFe<sub>2</sub>S<sub>3</sub> crystallizes within the cubic form. Rietveld refinements were therefore carried out using *F43m* space group. However, extra peaks and peak shoulders which may be attributed to the chalcopyrite phase can be observed (inset Fig. 1). Thus, from the refinements, the CuFe<sub>2</sub>S<sub>3</sub> isocubanite (around 72 wt% – 63 at%) is the majority phase, while the minority one is the chalcopyrite (around 28 wt% – 37 at%). The structural refinement leads to

<sup>†</sup> The product was characterized by XRD using a Philips X'Pert diffractometer with Bragg-Brentano geometry (CuK<sub>α1,2</sub> radiation). Note that due to their instability in air, the reduced phases XRD patterns were registered under vacuum using a chamber attached to a Bruker D8 diffractometer. Electrochemical characterizations of CuFe<sub>2</sub>S<sub>3</sub> have been performed in Swagelok cells. Metallic lithium (Aldrich, 99.9%) has been used as negative electrode, LP30 from Merck [1 M LiPF<sub>6</sub> in an ethylene carbonate/dimethyl carbonate 1 : 1 (w/w) Selectipur] was used as the electrolyte, and the positive electrode was constituted of approximately 10 mg of a mixture of the active material with 50% weight of carbon (acetylene black). The electrochemical cells were cycled at constant current between 1.2 and 3.0 V at different galvanostatic rates on a VMP II potentiostat/galvanostat (Biologic SA, Claix, France) at room temperature. Potentiostatic intermittent titration technique (PITT) measurements were conducted using a potential step of 10 mV limited by a minimum current equivalent to a C/10 galvanostatic rate.

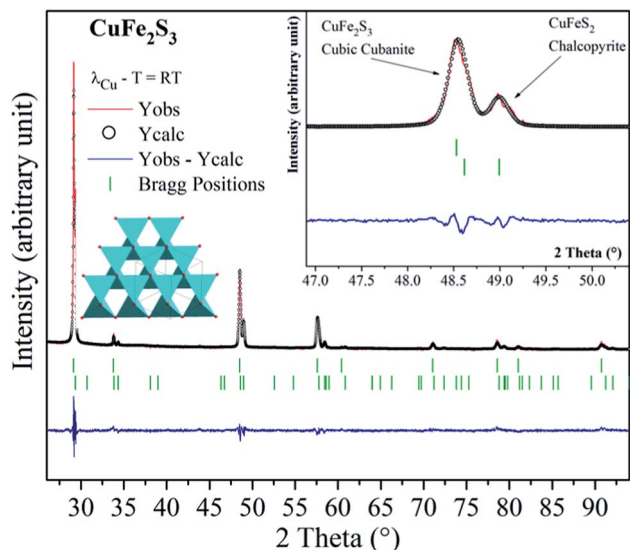


Fig. 1 Powder X-ray diffraction pattern of  $\text{CuFe}_2\text{S}_3$  isocubanite. Vertical bars, respectively, indicate the Bragg peak positions corresponding to the chalcopyrite  $\text{CuFeS}_2$  (bottom green bars – space group:  $I42d$  no. 122) and to the cubic cubanite so-called isocubanite  $\text{CuFe}_2\text{S}_3$  (top green bars space group:  $F43m$  no. 216). Inset shows a zoomed-in portion of the aforementioned figure, showing the coexistence of the  $\text{CuFe}_2\text{S}_3$  isocubanite and  $\text{CuFeS}_2$  chalcopyrite.

unit cell parameters  $a = 5.3018(1) \text{ \AA}$  and  $a = 5.2927(3) \text{ \AA}$ ,  $c = 10.4340 \text{ \AA}$  for the isocubanite and chalcopyrite phases, respectively. The aforementioned unit cell parameters are close to those reported in the literature and then confirms their good crystallinity.<sup>22</sup> The isocubanite structure can be described as a tetragonal close-packed stacking of  $\text{S}^{2-}$  anions, which occupy the  $4a$  (0, 0, 0) crystallographic site while Cu and Fe cations are randomly distributed over the two structurally equivalent tetrahedral sites  $4c$  ( $1/4, 1/4, 1/4$ ) and  $4d$  ( $3/4, 3/4, 3/4$ ). Different Rietveld refinements were therefore performed with both  $4c$  and  $4d$  crystallographic sites, and best result through low isotropic displacement parameters and reliability factors ( $\chi^2 = 2.303$  and  $R_{\text{Bragg}}$  factor = 6.98%) was obtained with all Cu and Fe atoms on the  $4d$  crystallographic site. Although the obtained sample is intergrown with chalcopyrite; as previously studied, the chalcopyrite phase forms submicronic domains, this isocubanite sample is well crystallized.<sup>21</sup> Note that the average particle size is about 1–2  $\mu\text{m}$  without any particular shape.

The charge–discharge profiles of  $\text{Li}/\text{CuFe}_2\text{S}_3$  (Fig. 2a) have been performed by a galvanostatic cycling at  $C/20/\text{Li}$  per formula unit (f.u.) in the potential window 0.5–3.0 V versus  $\text{Li}^+/\text{Li}$ . Starting from our material, the first discharge is fragmented in a series of two main processes happening between 1.80 and 0.50 V. The first one is a slope (A) from 1.80 to 1.50 V, it is attributed to the insertion of one lithium into  $\text{CuFe}_2\text{S}_3$  through a solid solution, accordingly to literature.<sup>15</sup> This insertion follows the eqn (1):

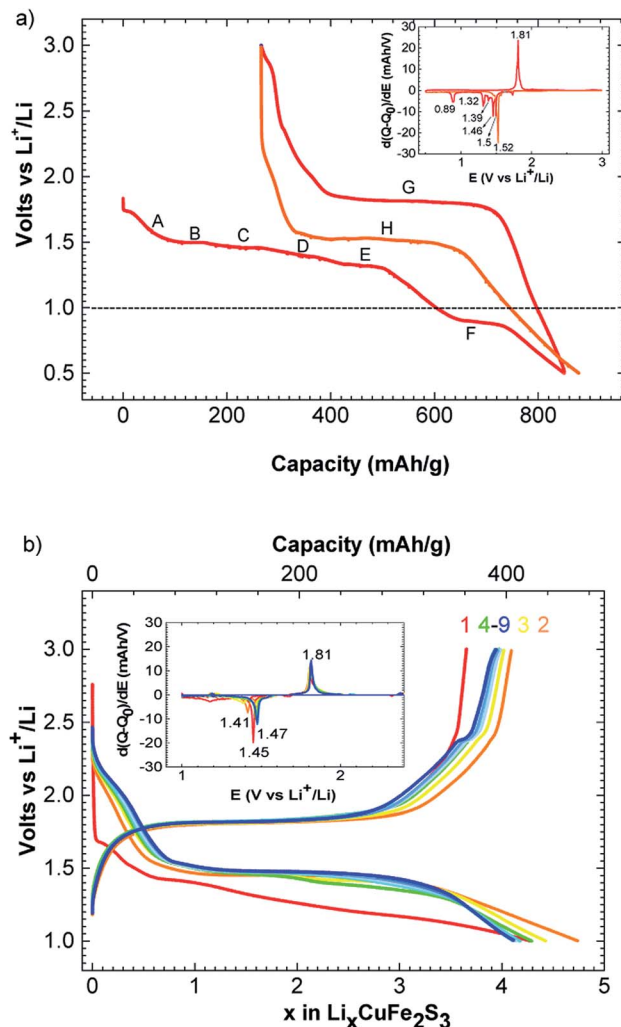
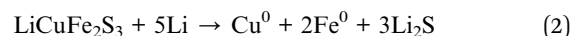


Fig. 2 Voltage–composition curve for  $\text{CuFe}_2\text{S}_3$  in the potential window 3.0–0.5 V at  $C/20/\text{Li}$  and inset: derivative curve  $|dQ/dE|$  vs. voltage (a); voltage–composition curve for  $\text{CuFe}_2\text{S}_3$  in the potential window 3.0–1.0 V at  $C/2/\text{Li}$  and its corresponding derivative curve  $|dQ/dE|$  vs. voltage (b).

Note that the phase  $\text{LiFeCuS}_2$  has been reported<sup>15</sup> and our sample is an intergrowth between chalcopyrite  $\text{CuFeS}_2$  and isocubanite  $\text{CuFe}_2\text{S}_3$ , a complete structural resolution of the lithiated phase is not possible. During the second process, we observe 5 plateaus at 1.50 (B), 1.46 V (C), 1.39 (D), 1.32 (E) and 0.82 (F) volt, respectively as shown on the derivative curve (inset Fig. 2a). These processes correspond to the reaction with 5 lithium and could then be assigned to copper and iron reduction to the metallic level as related in the case of  $\text{Li}/\text{CuFeS}_2$  system<sup>15</sup> following the eqn (2):



Because of the nature of our material (intergrowth of isocubanite and chalcopyrite), it is interesting to point out that only two domains are observed in the course of the first discharge of pure  $\text{CuFeS}_2$  phase (at 1.7 and 1.5 V, respectively<sup>16</sup>). Charging process occurs mainly through one plateau at 1.80 V

(G) as shown on the derivative curve (Red curve, Fig. 2b). This plateau could be attributed to copper and iron oxidation leading to a mixture of copper iron sulfides  $\text{Cu}_x\text{Fe}_y\text{S}_z$  (ref. 15, 23 and 24) and free sulfur formation. Consequently, this system becomes a hybrid between lithium ion and lithium sulfur battery. As observed on Fig. 2, the first discharge process is different than the second one where only one large plateau at 1.50 V (*H*) is observed. This can be due to SEI formation occurring at the same time than metal reduction in the first discharge. SEI formation has already been mentioned in similar conversion cathode study to be responsible for extra capacity like  $\text{CuFeS}_2$ ,<sup>15</sup>  $\text{Co}_2\text{SiO}_4$  (ref. 25) and  $\text{CuCo}_2\text{S}_4$ .<sup>26</sup> In our case, an extra capacity of  $260 \text{ mA h g}^{-1}$  is observed. We particularly have to consider the presence of  $\text{CuFeS}_2$  in our material.  $\text{CuFeS}_2$  has been previously investigated and possesses similar electrochemical properties compare to  $\text{CuFe}_2\text{S}_3$ . Even if our material contains a large amount of  $\text{CuFeS}_2$ , the electrochemical capacity cannot only be due to  $\text{CuFeS}_2$  activity. Therefore, this indicates that  $\text{CuFe}_2\text{S}_3$  is an electroactive material.

A reversible capacity of  $560 \text{ mA h g}^{-1}$  (C/20/Li) is observed in the potential window of 1.52 V to 1.80 V. Please, note that an additional phenomenon appears below 1.50 V. This latter could correspond to different phenomena like electrolyte degradation or lithium insertion in the surface electrolyte interface as mentioned in previous report.<sup>27,28</sup> We believe that the irreversible capacity is mainly ascribed to this slope and the SEI formation.

Study at a rate of C/2/Li and a cut off at 1.0 V are displayed Fig. 2b. The curve of C/2/Li shows a reversible and stable capacity of  $400 \text{ mA h g}^{-1}$  upon 9 cycles. Using this rate, a polarization of 340 mV is observed between formation and conversion of  $\text{Cu}_x\text{Fe}_y\text{S}_z$ . This polarization is quite in accordance with previous electrochemical performance obtained for  $\text{CuFeS}_2$ .<sup>17</sup> We can notice that cutting off at 1.0 V improves the reversibility of the system. Note that the conversion process is not complete as last discharge plateau at 0.82 V is also cutted off. Consequently, first reduction plateaus appeared at lower voltage and then stabilized at 1.47 V after few cycles (Fig. 2b).

The intermittent galvanostatic titration (GITT) reported in Fig. 3a shows a biphasic process and allows us to access to the equilibrium potential in the course of the reduction with a thermodynamic potential of 1.65 V vs.  $\text{Li}^+/\text{Li}$ . A polarization of 300 mV is observed. The potentiodynamic titration curve (PITT, Fig. 3b) reveals a bell-shape-type response on the reversible phenomenon, and confirms together with the sharpness of the peaks in the derivative curve (Fig. 2) that the reversible process is biphasic.

To confirm the structural conversion occurring in the course of the electrochemical process, *ex situ* X-ray diffraction patterns have been recorded at the end of the first discharge and charge (Fig. 4). We can see on the discharge pattern that  $\text{CuFe}_2\text{S}_3$  reflections disappeared (green middle curve, Fig. 4). Reflections on discharge pattern are attributed to copper ( $\circ$ ), iron ( $\Delta$ ) and  $\text{Li}_2\text{S}$  ( $+$ ). After recharge (orange upper curve, Fig. 4), reflection close to  $\text{CuFe}_2\text{S}_3$  and attributed to  $\text{Cu}_x\text{Fe}_y\text{S}_z$  (\*) are observed among undefined products ( $\square$ ). This validates the conversion mechanism.

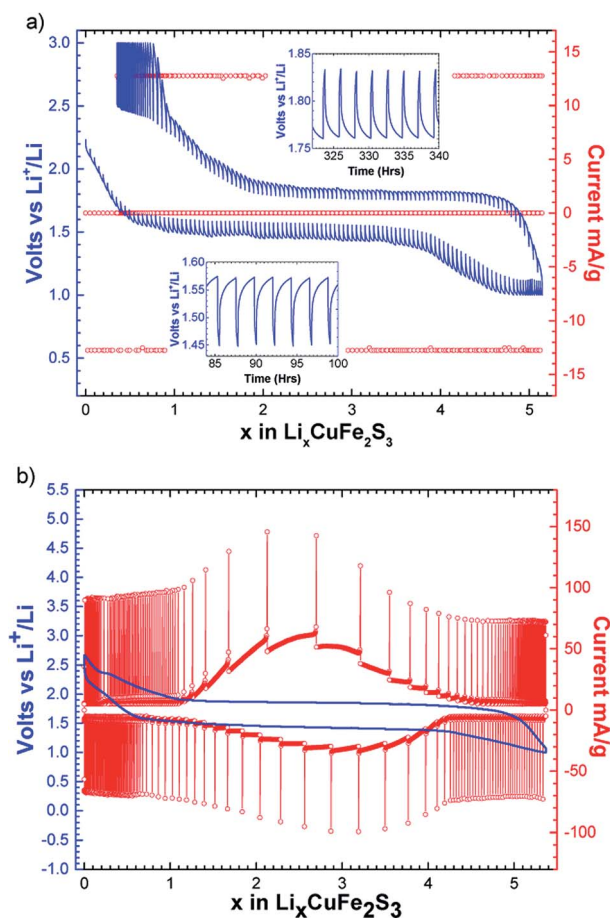


Fig. 3 (a) Potential–composition curve of  $\text{CuFe}_2\text{S}_3$  performed in a galvanostatic intermittent mode (GITT) with a rate of C/40 for 15 min and relaxation period of 2 h, (b) potentiometric titration curve (PITT) in the range of 3.0–1.0 V vs.  $\text{Li}^+/\text{Li}$  using 5 mV potential step in duration of 1 h and current limitation equivalent to a galvanic current  $I_{\text{limit}} = I_{\text{C}/100}$ .

The specific capacity decreases with the increase in current density (Fig. 5a). The reversible capacity is about  $425 \text{ mA h g}^{-1}$  at the current density of C/5/Li and decreases down to  $30 \text{ mA h g}^{-1}$  at 10C/Li. When the current density is tuned back at C/5/Li, the specific capacity rebounds to  $350 \text{ mA h g}^{-1}$ . This

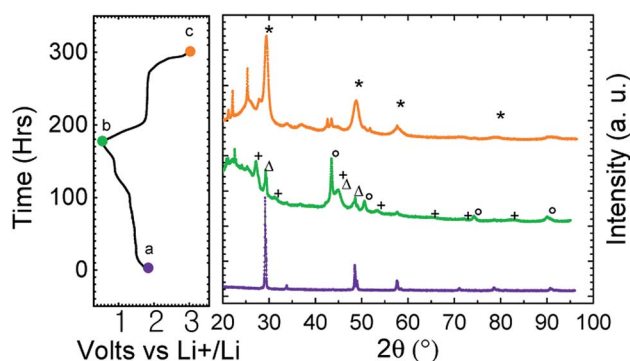


Fig. 4 Powder X-ray diffraction patterns of (a) as prepared isocubanite  $\text{CuFe}_2\text{S}_3$ , (b) discharged phase down to 0.5 V (C/20) (c) charged phase up to 3.0 V (C/20).  $\text{Cu}_x\text{Fe}_y\text{S}_z$  (\*),  $\text{Li}_2\text{S}$  (+), Cu ( $\circ$ ), Fe ( $\Delta$ ) and undefined products ( $\square$ ).





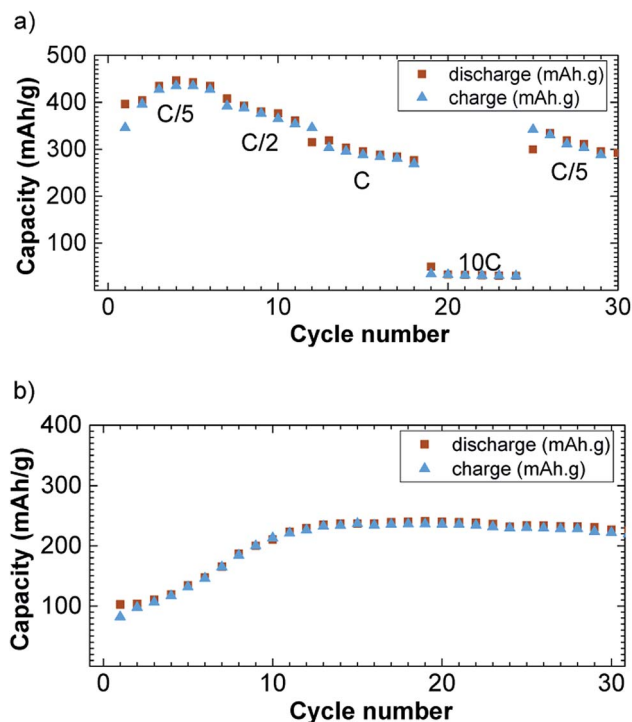


Fig. 5 Rate (a) and cycling (b) capability versus cycle number at C/Li in 1.2–3.0 V potential window for the discharge (brown square) and charge (blue triangle) capacity versus cycle number.

rate capability is comparable with previously reported  $\text{CuFeS}_2$  rate capabilities.<sup>17</sup> Please note that we observed a capacity fading, which appeared to be not rate depending, and could be attributed to polysulfides formation known to be formed in lithium sulfur battery.<sup>8</sup> Those polysulfides are the results of  $\text{Li}_2\text{S}$  reduction that can form free sulfur.

On Fig. 5b, we have reported the cycling performances of  $\text{CuFe}_2\text{S}_3$  at a current density of C/Li upon 30 cycles and with a cut off at 1.2 V. The cut off was necessary to avoid side reactions to occur as observed on the potential slope observed at the end of the first discharge. The capacity is rising in the first 10 cycles from 100 to 245  $\text{mA h g}^{-1}$  and stabilizes around 250  $\text{mA h g}^{-1}$ . We believe this is due to the incomplete reaction together with side reaction despite the high voltage cut off.

The electrochemical behaviour of  $\text{CuFe}_2\text{S}_3$  and  $\text{CuFeS}_2$  are relatively close to each other's. Their working potential is around 1.8 V and similar phenomena (conversion process, SEI formation, extra electrochemical capacity) are observed for both compounds. Furthermore, they are both semi-conductors. Concerning resistivity, our isocubanite sample (containing chalcopyrite) owns a resistivity of 0.7 mohm cm at 300 K while pure chalcopyrite possesses a higher resistivity at room temperature (measured between 20 and 200 mohm cm).<sup>29</sup>

## Conclusions

In this work, we demonstrate the conversion of the intergrowth between the two phases  $\text{CuFe}_2\text{S}_3$  and  $\text{CuFeS}_2$  into  $\text{Li}_2\text{S}$  and native copper and iron particles. Moreover, *ex situ* XRD at the

end of the charge showed that a new phase  $\text{Cu}_x\text{Fe}_y\text{S}_z$  is formed. This new phase showed common diffraction peaks with the starting intergrowth but a complete structural resolution is not possible due to the low crystallinity of the material. More importantly, a reversible capacity of 425  $\text{mA h g}^{-1}$  at a C/5/Li rate upon 10 cycles and with a cut off at 1.0 V is obtained. The redox potential of 1.65 V vs.  $\text{Li}^+/\text{Li}$  gives an energy density of 600  $\text{W h kg}^{-1}$ . This result points out that despite the intergrowth nature of the material between isocubanite and chalcopyrite, we obtain comparable performance for this family of materials.

## Conflicts of interest

There are no conflicts to declare.

## Notes and references

- 1 K. Zhang, T. Zhang, J. Liang, Y. Zhu, N. Lin and Y. Qian, *RSC Adv.*, 2015, **5**, 14828–14831.
- 2 B. Jache, B. Mogwitz, F. Klein and P. Adelhelm, *J. Power Sources*, 2014, **247**, 703–711.
- 3 A. Débart, L. Dupont, R. Patrice and J.-M. Tarascon, *Solid State Sci.*, 2006, **8**, 640–651.
- 4 S.-C. Han, H.-S. Kim, M.-S. Song, P. S. Lee, J.-Y. Lee and H.-J. Ahn, *J. Alloys Compd.*, 2003, **349**, 290–296.
- 5 Y. Uetani, K. Yokoyama and O. Okamoto, *J. Power Sources*, 1980, **5**, 89–98.
- 6 H. Mukaibo, A. Yoshizawa, T. Momma and T. Osaka, *J. Power Sources*, 2003, **119–121**, 60–63.
- 7 J. Wang, G. Wang, L. Yang, S. H. Ng and H. Liu, *J. Solid State Electrochem.*, 2006, **10**, 250–254.
- 8 J. Cabana, L. Monconduit, D. Larcher and M. R. Palacín, *Adv. Mater.*, 2010, **22**, E170–E192.
- 9 F. Bonino, M. Lazzari, B. Rivolta and B. Scrosati, *J. Electrochem. Soc.*, 1984, **131**, 1498–1502.
- 10 J.-S. Chung and H.-J. Sohn, *J. Power Sources*, 2002, **108**, 226–231.
- 11 X. Feng, X. He, W. Pu, C. Jiang and C. Wan, *Ionics*, 2007, **13**, 375–377.
- 12 J.-W. Choi, G. Cheruvally, H.-J. Ahn, K.-W. Kim and J.-H. Ahn, *J. Power Sources*, 2006, **163**, 158–165.
- 13 H. Siyu, L. Xinyu, L. QingYu and C. Jun, *J. Alloys Compd.*, 2009, **472**, L9–L12.
- 14 S.-H. Kim, Y.-J. Choi, D.-H. Kim, S.-H. Jung, K.-W. Kim, H.-J. Ahn, J.-H. Ahn and H.-B. Gu, *Surf. Rev. Lett.*, 2008, **15**, 35–40.
- 15 P. Guo, H. Song, Y. Liu and C. Wang, *ACS Appl. Mater. Interfaces*, 2017, **9**, 31752–31762.
- 16 W. Ding, X. Wang, H. Peng and L. Hu, *Mater. Chem. Phys.*, 2013, **137**, 872–876.
- 17 X. Wu, Y. Zhao, C. Yang and G. He, *J. Mater. Sci.*, 2015, **50**, 4250–4257.
- 18 Y. Wang, X. Li, Y. Zhang, X. He and J. Zhao, *Electrochim. Acta*, 2015, **158**, 368–373.
- 19 M. E. Fleet, *Z. Kristallogr.*, 1970, **132**, 276–287.



- 20 S. Pareek, A. Rais, A. Tripathi and U. Chandra, *Hyperfine Interact.*, 2008, **186**, 113–120.
- 21 T. Barbier, D. Berthebaud, R. Frésard, O. I. Lebedev, E. Guilmeau, V. Eyert and A. Maignan, *Inorg. Chem. Front.*, 2017, **4**, 424–432.
- 22 J. T. Szymasski, *Acta Crystallogr.*, 1974, **140**, 240–248.
- 23 S.-B. Son, T. A. Yersak, D. M. Piper, S. C. Kim, C. S. Kang, J. S. Cho, S.-S. Suh, Y.-U. Kim, K. H. Oh and S.-H. Lee, *Adv. Energy Mater.*, 2014, **4**, 1300961.
- 24 L. Li, M. Cabán-Acevedo, S. N. Girard and S. Jin, *Nanoscale*, 2014, **6**, 2112–2118.
- 25 F. Mueller, D. Bresser, N. Minderjahn, J. Kalhoff, S. Menne, S. Krueger, M. Winter and S. Passerini, *Dalton Trans.*, 2014, **43**, 15013–15021.
- 26 L. Nie, H. Wang, Y. Chai, S. Liu and R. Yuan, *RSC Adv.*, 2016, **6**, 38321–38327.
- 27 S. Grugeon, S. Laruelle, L. Dupont and J.-M. Tarascon, *Solid State Sci.*, 2003, **5**, 895–904.
- 28 S. Laruelle, S. Grugeon, P. Poizot, M. Dollé, L. Dupont and J.-M. Tarascon, *J. Electrochem. Soc.*, 2002, **149**, A627.
- 29 R. Lefèvre, D. Berthebaud, M. Y. Mychinko, O. I. Lebedev, T. Mori, F. Gascoin and A. Maignan, *RSC Adv.*, 2016, **6**, 55117–55124.

